Dependence of the shattered-pellet-mitigated thermal quench radiation efficiency on the plasma thermal energy in DIII-D

R. Sweeney[1], R. Raman[2], N. Eidietis[3], J. Herfindal[4], E. Hollmann[5], D. Hu[1], M. Lehnen[1], D. Shiraki[4], J.A. Snipes[1]

[1] *ITER Organization, Route de Vinon-sur-Verdon - CS 90 046 - 13067 Saint Paul-lez-Durance Cedex, France*
[2] *University of Washington, Seattle, WA 98195, USA*
[3] *General Atomics, PO Box 85608, San Diego, CA 92186-5608, USA*
[4] *Oak Ridge National Laboratory, Oak Ridge, TN 37831, USA*
[5] *University of California-San Diego, 9500 Gilman Dr., La Jolla, CA 92093-0417, USA*

Unmitigated disruptions in ITER can produce significant melting and evaporation, and apply forces to the first wall and vessel [1]. Techniques to inject high-Z noble gases have been employed in existing tokamaks to mitigate disruption forces and heat loads [2]. Shattered pellet injection (SPI) is expected to deliver deuterium and impurities further into the core of reactor-scale fusion plasmas than gas injection techniques, and is the approach adopted for the ITER disruption mitigation system [3]. As DIII-D is presently the only tokamak with an operational SPI, investigating large variations of plasma parameters is important for first predictions of the system performance in ITER.

Thermal quench (TQ) SPI mitigation experiments were conducted in the Super H-mode scenario ($W_{th} = 1.9$ MJ) and compared with a previously studied H-mode scenario ($W_{th} = 0.78$ MJ) [4]. It is found here that the conventional tokamak radiation diagnostics are insufficient to confirm the $> 90\%$ TQ radiation efficiency required for the ITER $Q = 10$ scenario. Toroidal radiation asymmetries in the Super H-mode are presented and qualitative comparisons of the radiation efficiency between the two experimental scenarios are discussed. Radiation measurements from the Absolute eXtreme UltraViolet (AXUV) diodes and the foil bolometers are presented, and uncertainties due to time-resolution, limited measurement dimensionality, and diode sensitivity are discussed. Potential upgrades to the radiation diagnostics for these measurements are proposed.

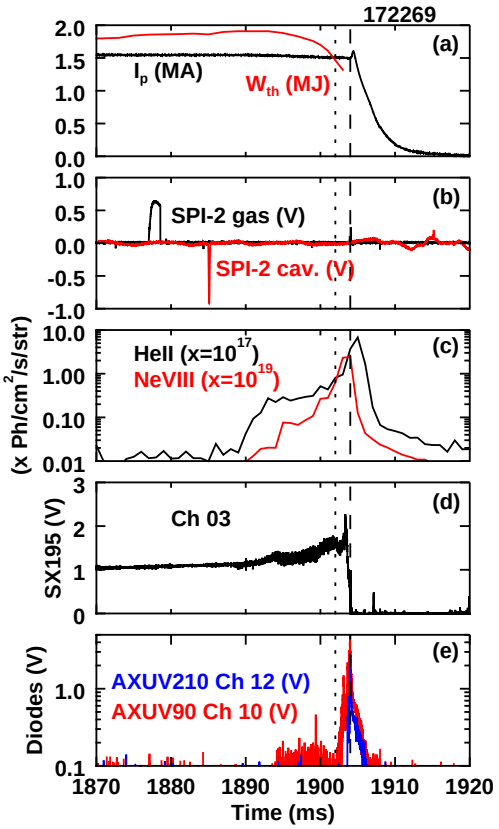

Figure 1: *Evolution of discharge 172269 during the injection of a pure 7 mm Ne pellet.*

An example Super H-mode discharge is shown in Fig. 1 reaching a maximum thermal energy of $W_{th} = 1.9$ MJ (Fig. 1a, red). The plasma current enters the "flat-top" phase and the edge saftey factor reaches $q_{95} = 4$ before the pellet is propelled by pressurized helium at 1876 ms (Fig. 1b, black). The pellet is observed traversing the microwave cavity $\sim$10 ms later (Fig. 1b, red). The pellet is shattered into a plume of small solid fragments, liquid, and gas by a bend in the barrel. The plume enters the vessel at $\phi = 135^\circ$ and $\theta \approx 45^\circ$, and the fast camera detects the first NeI line radiation at $t = 1902.97 \pm 0.05$ ms, indicated by the vertical dotted lines in each subpanel. Before the plume arrival, helium propellant gas and some entrained Ne reach the plasma, as evidenced by the HeII and NeVIII line radiation (Fig. 1c). This early gas delivery

causes a ∼20% decrease in thermal energy (Fig. 1a). Following arrival of the plume at the plasma separatrix, a transient spike is observed in the core soft X-ray channel (Fig. 1d) at a time consistent with the flight time to the $q = 2$ surface at a speed of 203 m/s. The soft X-ray signal subsequently collapses to 10% of the peak in 750 μs. These Super H-mode discharges are compared with previously reported Ne SPI terminated H-mode discharges [4]. Important differences of the H-mode include the location of the injection at $\phi = 15^\circ$ and $\theta \approx 45^\circ$, a lower edge safety factor of $q_{95} = 3.2$, and a lower thermal energy of $W_{th} = 0.78$ MJ.

Radiated power measurements are made in DIII-D using two 24-channel foil bolometer arrays with views from the upper and lower outboard wall at $\phi = 75^\circ$ and $\phi = 60^\circ$ respectively, and using three AXUV diode fan arrays, consisting of two 32-channel arrays with views from the upper and lower outboard wall at $\phi = 90^\circ$, and one 30-channel array on the upper outboard wall at $\phi = 210^\circ$ (see [5] Fig. 1). Resolving the emitting region in 3D is important for accurate radiated power measurements. The radiated power from a toroidally elongated source falls off like $(lR_s)^{-1}$, where l is the distance from the diode to the source and R_s is the major radius at the source location [6]. Since the diodes are located on the outboard side, R_s varies inversely with l and partially compensates the spatial dependence, but in the most extreme cases, errors of 200-300% in measured power are possible when the location of the source is unknown (see Fig. 2 of [6]).

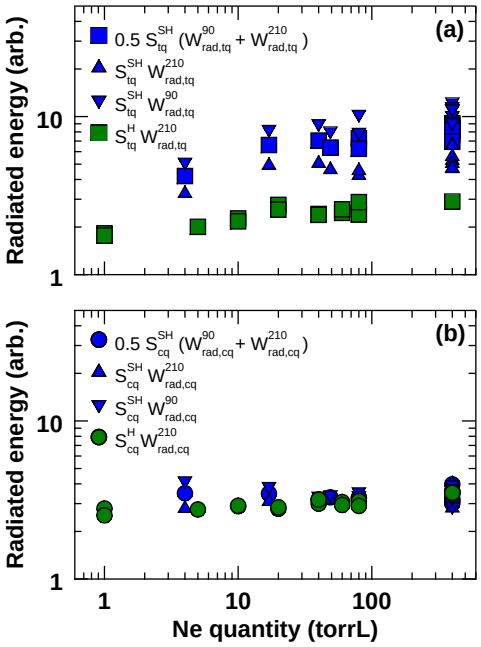

Figure 2: *Single fan array AXUV inversions in H- (green) and Super H-mode (blue) during (a) the thermal quench, and (b) the current quench.*

In addition, the responsivity of the AXUV diodes varies by 200% for photons between 5 eV and 100 eV (see Fig. 2 of [7]). The electron temperature during a Ne mitigated TQ in DIII-D drops from the keV range to ∼ 10 eV by the start of the CQ, and thus radiation is expected where the responsivity depends strongly on photon energy.

During the Super H-mode discharges, the lower AXUV fan array at $\phi = 90^\circ$ was high-pass filtered for soft X-ray measurements, and during the H-mode discharges, the upper and lower were filtered. Measurements from a single fan array provide the radiated power in one-dimension, and require an assumption on the radiation distribution to invert them. The pre-disruption separatrix geometry is segmented in the poloidal direction into radially thin, independent radiation cells, and the emissivity of the cells are best-fit to reproduce the line integrated AXUV chord measurements. The inversions are then time-integrated to estimate the radiated energy.

The radiated energies during the TQ and CQ in the Super H-mode (SH) and the H-mode (H) are shown as a function of the pellet Ne quantity in Fig. 2. The radiated powers are time-integrated over the 10 ms before the current spike, and separately during the 15 ms following the current spike. To account for the diode sensitivity, a factor S might be used during the TQ and the CQ to convert the arbitrary units to energy. Due to differences in the plasma thermal energy, and to exposure of the diodes to neutron and UV fluences, the S factors are not necessarily the same for the H- and the Super H-mode discharges. The AXUV210 array should not be directly compared between the two scenarios due to considerations of toroidal asymmetries and the

different injection locations. An increasing TQ radiated energy is observed with increasing Ne quantity in both scenarios (Fig. 2a). The trend appears stronger in the Super H-mode, which might suggest that the thermal mitigation efficieny for small Ne quantities is lower than in the H-mode, or alternatively, that the pure Ne pellet mitigation is better in the Super H-mode. The CQ radiated energies are approximately constant with Ne quantity in the Super H-mode, whereas a marginal increase in the H-mode radiation with increasing Ne quantity is observed (Fig. 2b), which might imply that the CQ is not fully mitigated for low quantities of Ne.

The TQ radiated energies measured at $\phi = 90^\circ$ are consistently larger than the measurements at $\phi = 210^\circ$ in the Super H-mode (Fig. 2). The radiated energy at $\phi = 90^\circ$ normalized by the average radiated energy is shown in Fig. 3, and provides a lower bound on the toroidal peaking factor. Higher toroidal radiation peaking is sometimes observed for larger Ne quantities, but a large Ne quantity does not necessarily imply a high toroidal peaking. The toroidal asymmetry in the H-mode discharges is unknown since the radiated power data at $\phi = 90^\circ$ are unavailable.

The upper and lower bolometer fan arrays can measure spatial distributions of radiation evolving with a timescale of ~ 8 ms in one toroidal location [8]. This time resolution prohibits resolving the small-scale TQ structures from the more uniform distributions expected during the CQ, and requires integrating the radiated power over both the TQ and CQ. To normalize the total radiated energy $W_{\rm rad}$, it is necessary to estimate the total magnetic energy that is deposited on the wall by radiation. Here we make the conservative estimate that the vessel is ideal, and thus only the magnetic energy inside the vessel, $W_{\rm mag,in}$, is dissipated by the plasma. The ideal vessel assumption was also used in [9] where it is posited that the poloidal field coils form a conducting "coil-cage", resulting in a significantly longer resistive diffusion time for axisymmetric fields than the typical 5 ms timescale used for non-axisymmetric fields. The ideal wall assumption is used here, though validation of the coil-cage is still in progress.

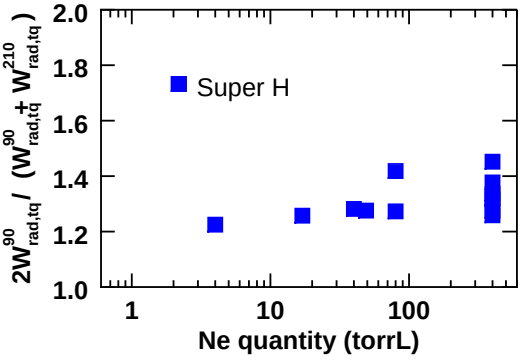

Figure 3: *Lower bound on the toroidal peaking factor during the TQ as a function of the pellet Ne quantity.*

A tomographic inversion of the 2D bolometer data is performed and an estimate of the total radiated energy is found. The inferred radiated fraction, $f_{\rm rad} = W_{\rm rad}/(W_{\rm th} + W_{\rm mag,in})$, as a function of the thermal fraction, $f_{\rm th} = W_{\rm th}/(W_{\rm th} + W_{\rm mag,in})$, is shown in Fig. 4. If we assume that the errors resulting from the time-resolution of the bolometers are small, then there are at least two interpretations of Fig. 4. If we assume that in the Super H-mode, the toroidal peaking factor is no larger than 1.5 (see Fig. 3) and peaked at the location of the bolometer array, and if we assume the CQ mitigation efficiency is near 100%, then the best mitigated discharges in Fig. 4 suggest 35% TQ mitigation using pure Ne pellets (a value of $W_{mag,in} = 2$ MJ is used here). If we assume that the radiation is axisymmetric in the H-mode (since there is no knowledge of the asymmetry) and that the CQ is fully mitigated, the data in Fig. 4 suggest 20% TQ mitigation for pure Ne pellets (a value of $W_{mag,in} = 1$ MJ is used here). If instead we assume that the TQ radiation is strongly toroidally peaked at a location not viewed by the bolometer, then the data might be consistent with good thermal mitigation efficiency, albeit with a high toroidal peaking factor. The error bars in Fig. 4 reflect the large uncertainty in this measurement.

To assess the TQ radiation efficiency for ITER, radiation diagnostic improvements are necessary at all participating tokamaks. Locating bright spots in the poloidal plane to within many

centimeters and with sub-millisecond time-resolution is necessary. Many poloidal cross-sections of the emissivity within a small toroidal sector centered about the SPI are required to resolve the evolution of the radiating plume in 3D, and additional poloidal cross-sections are needed at other toroidal angles to resolve larger scale structures. Each poloidal plane diagnostic might consist of dual (or many) view AXUV diode fan arrays, and dual (or many) view bolometer fan arrays. The sub-millisecond evolution of the emitting structure from the AXUV arrays can be scaled by a parameterized, best-fit radiation power time-trace to reconstruct the slower ($\sim$ 1 ms) measurements of the colocated bolometers. Alternatively, each poloidal plane diagnostic set might consist of three redundant AXUV arrays, with different filters for the three dominant spectral sensitivity bands, allowing for proper absolute radiated energy measurements. Interpolating and integrating between each toroidally localized energy measurement would provide an improved total radiated energy. The JOREK code with the new SPI impurity model [D. Hu et al., P4.1043, this conference] is well suited to assess the accuracy of this proposed diagnostic.

Super H-mode discharges, and previously reported H-mode discharges [4], were terminated using Ne shattered pellets in DIII-D to inform predictions of the TQ radiation efficiency in ITER. In the Super H-mode discharges, helium propellant and entrained Ne are observed to reach the plasma and reduce the thermal energy by $\sim$ 20% before arrival of the shattered material. Using the AXUV diodes, the energy radiated during the TQ is observed to increase as the quantity of injected Ne increases in both scenarios. The trend appears stronger in the Super H-mode discharges, which could imply better radiation efficiency with pure Ne pellets in the Super H-mode, or lower radiation efficiency when injecting pure D2 pellets. A lower bound measurement of the toroidal radiation peaking indicates that high toroidal peaking may, but not necessarily, occur for large injected Ne quantities. The AXUV diagnostics in these experiments provide only 1D measurements of the emission, and vary in sensitivity by up to 200% over the range of expected photon energies. Using the bolometers, the total radiated energies in both scenarios might suggest low TQ radiation efficiency, or good TQ radiation efficiency with high toroidal peaking of the radiation. The time resolution of the bolometers is low relative to the TQ duration, prohibiting accurate reconstructions of the emission. A diagnostic upgrade capable of validating the $>$ 90% TQ radiation efficiency is proposed, and the JOREK code with an SPI impurity model and a synthetic diagnostic might be used to optimize the design.

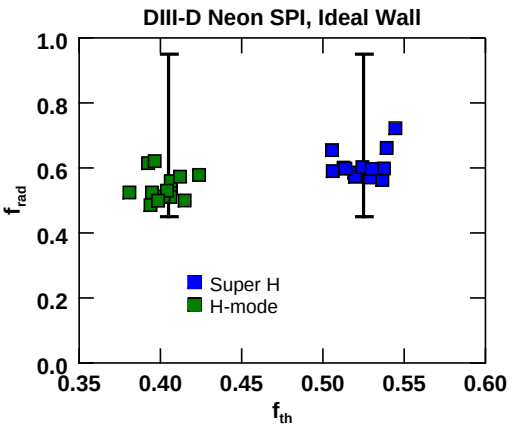

Figure 4: *TQ mitigation performance f_{rad} as a function of the thermal fraction. In each scenario, the pellet mixtures range from pure D2 to pure Ne (same discharges as Fig. 2).*

Acknowledgments: This material is based upon work supported by the U.S. Department of Energy, Office of Science, Office of Fusion Energy Sciences, using the DIII-D National Fusion Facility, a DOE Office of Science user facility, under Awards DE-FC02-04ER54698. DIII-D data shown in this paper can be obtained in digital format by following the links at https://fusion.gat.com/global/D3D_DMP. **Disclaimer:** This report was prepared as an account of work sponsored by an agency of the United States Government. Neither the United States Government nor any agency thereof, nor any of their employees, makes any warranty, express or implied, or assumes any legal liability or responsibility for the accuracy, completeness, or usefulness of any information, apparatus, product, or process disclosed, or represents that its use would not infringe privately owned rights. Reference herein to any specific commercial product, process, or service by trade name, trademark, manufacturer, or otherwise does not necessarily constitute or imply its endorsement, recommendation, or favoring by the United States Government or any agency thereof. The views and opinions of authors expressed herein do not necessarily state or reflect those of the United States Government or any agency thereof, or the ITER Organization.

References

[1] M. Lehnen et al., J. Nucl. Mater. **463**, 39-48 (2015)
[2] E.M. Hollmann et al., Phys. Plasmas **22**, 021802 (2005)
[3] L.R. Baylor et al., IEEE Trans. Plasma Sci. **44**, 9 (2016)
[4] D. Shiraki, N. Commaux et al., Phys. Plasmas **23**, 062516 (2016)
[5] E.M. Hollmann, T.C. Jernigan, P.B. Parks et al., Nucl. Fusion **48**, 115007 (2008)
[6] D.S. Gray et al., Rev. Sci. Instrum. **75**, 10 (2004)
[7] D.S. Gray et al., Rev. Sci. Instrum. **75**, 2 (2004)
[8] A.W. Leonard, W.H. Meyer, B. Geer, D.M. Behne, and D.N. Hill, Rev. Sci. Instrum. **66**, 1201-1204 (1995)
[9] A.W. Hyatt, R.L. Lee, et al. 23rd EPS Conference vol. 20C, Kiev, Ukraine (1996)